Re-evaluation of the sequential 3α reaction in stellar conditions

Theodoros Depastas[1,*], *Shuting* Sun[2], *Hongbin* He[2], *Hua* Zheng[2], and *Aldo* Bonasera[1,3]

[1]Cyclotron Institute, Texas A&M University, College Station, Texas 77840, USA
[2]School of Physics and Information Technology, Shaanxi Normal University, Xi'an 710119, China
[3]Laboratori Nazionali del Sud, INFN, Catania 95123, Italy

Abstract. The formation of carbon via the triple alpha process is a key step in stellar production reactions of light ions and heavily impacts the life-cycle of red giant stars. Here, we propose a novel theoretical approach for sequential mechanism of the helium burning process, based on the Imaginary Time Method (ITM) and semi-classical models. We compare our results to those of the NACRE collaboration, which has set the standard for the past decades. Our calculations differ by several orders of magnitude in the low temperature region, which may seriously affect the early evolution of helium burning stars.

The triple alpha process was the stage point for the development of the theory Stellar Nucleosynthesis in the early 1950's by Fowler, Hoyle and Saltpeter [1–3]. Since then, it has been discussed extensively in the literature, for both its nuclear [4–10] and astrophysical [11–14] aspects.

Astrophysically, helium burning comes after the hydrogen burning in main sequence stars[13], at temperatures of $\sim$ 0.1 GK [12]. This evolves them to the Red Giant and Asymptotic Giant Branch (AGB) phases [11], whose observable parameters constrain the reaction rates [14]. This process can also affect exotic dynamics, such as Type I supernovae and X-ray bursts in accreting White Dwarfs [15].

From the nuclear point of view, the formation of carbon proceeds through the tripe alpha process, mediated via the interaction of three α particles. The reaction rates are fine tuned by the presence of two resonances, the $E_{^8Be}$ = 92.08 keV, $\Gamma^{(0)}_{\alpha,Be}$ = 5.6 eV [5] ground state of ^{8}Be and the excited E_H = 7.654 MeV [2], $\Gamma^{(0)}_{\alpha,H}$ = 9.3 eV [16] Hoyle state of ^{12}C. The excited carbon decays via two γ transitions, firstly with $\Gamma^{(0)}_{\gamma,H}$ = 5.1 meV to the 2^+, 4.43 MeV state and then to the 0^+ ground state. Since the 2^+, 4.43 MeV state is below the α separation threshold, the second γ decay takes place without competition. The exact mechanism of this reaction is still a point of contention, with main candidates, the sequential [5, 15] and the direct three-body [6, 9, 10] reactions. Although both of these take place in a stellar environment, here we focus on the former mechanism. The validity of the direct three-body channel is discussed in Ref. [14] in terms of the compatibility of its results to astrophysical observations.

The sequential approach consists of two α particles forming an unstable ^{8}Be intermediate which then captures the third α, according to [11] :

$$\alpha + \alpha \rightarrow {}^8Be^*$$
$$\alpha + {}^8Be^* \rightarrow {}^{12}C + \gamma + \gamma'.$$

The first step inputs a threshold on the energy of the reactants at $Q_1 = -E_{^8Be}$. This feature is critical to the evaluation of the excited rates as we explain below. The total reaction rate is given by [5]:

$$R_{3\alpha} = \frac{\rho_\alpha^3}{3!}\langle\alpha\alpha\alpha\rangle, \tag{1}$$

with ρ_α being the number density of α's. The quantity $\langle\alpha\alpha\alpha\rangle$ corresponds to the reduced reaction rate, i.e., the reaction rate per triplet and encloses all the physical information of the system. For the past two decades, the methodology given by the NACRE collaboration [5, 8] has been a staple in the community for calculating the reduced rate. Here, we propose a novel theoretical framework and comment on the mathematical structure of the NACRE methodology. We denote these formulas with an index 'N'.

The first ingredient of our model is the sub-barrier fusion of the α particles and beryllium-8. The corresponding cross sections are calculated via the use of the semi-classical Hybrid α-Clustering (HαC) [17] or the Neck Model (NM) [18]. The HαC model, which has already been used [17, 19] to study astrophysical fusions, is a molecular dynamics approach. Its fundamental degrees of freedom are α particles interacting via the microscopic Hamiltonian [17]:

$$H = V_B + V_C + E_F, \tag{2}$$

where V_C and V_B are the Coulomb and Bass [20] potentials, respectively. The E_F is the Effective Fermi energy, that simulates the Heisenberg and Pauli correlations of the

*e-mail: tdepastas@tamu.edu

inner nucleons of the alpha particles, during their overlap. This is given by [17]:

$$E_F = 4x_F\bar{\epsilon}_F\rho^{2/3}, \tag{3}$$

with $\bar{\epsilon}_F = 21$ MeV, being the average Fermi energy of Nuclear Matter and the 2-Body density, $\rho = 2e^{-\beta(r/r_\alpha)^2}$, $r_\alpha = r_0 4^{1/3}$, $r_0 = 1.15$ fm. The constants x_F and β define the α-α potential and are fitted to experimental data. Here, we show two possible parameterizations, the standard one that is fitted to the binding energy of the ^{12}C ground state [17] and the other one that is fitted to the ^{8}Be resonance. In the subsequent text, it is assumed that we use the standard parameterization, unless specified otherwise.

The NM [18] is a mean-field description of the dynamical problem, based on the assumption that both fusing and fissioning nuclei are forming a Neck, in order to conserve their total volume [21]. The Winger transformation of the Time-Dependent Hartee-Fock equation for the evolution of the neck radius, leads to macroscopic Vlassov-like equations of motion, under the influence of the Coulomb, nuclear and neck-based friction interactions. For the nuclear interaction, we use a modification of the Bass potential that is tuned to reproduce the resonant states of the compound nucleus [22].

To simulate the tunneling below the Coulomb barrier, we employ the Imaginary Time Method (ITM) [23], which is discussed extensively in Refs. [19, 22–26]. In essence, the ITM forces the system to evolve in imaginary time between the two classical turning points, via the transformation, $t \rightarrow t = i\tau$. This reverses the sign of the collective nucleus-nucleus force [23] and allows the penetration of the barrier. The classical action in imaginary time (A), is correlated to the penetrability for a specific l-value (T_l), as follows [19, 23]:

$$T_l(E) = \begin{cases} \left(1 + e^{2A/\hbar}\right)^{-1} & , l = 0 \\ T_0\left(E - \frac{l(l+1)\hbar^2}{2\mu R_N^2}\right) & , l > 0 \end{cases}, \tag{4}$$

with R_N the channel radius. The corresponding cross sections, are then given by [23]:

$$\sigma_f(E) = \frac{\pi\hbar^2}{2\mu E}\sum_{l=0}^{\infty}(2l+1)T_l(E)(1+\delta_{12}), \tag{5}$$

where the $\delta_{12} = 1$ for identical nuclei and the sum is evaluated only at even and odd l-values, for identical bosons and fermions, respectively.

The fusion cross sections for both steps of the 3α process, are calculated via Eq. 5 for $l = 0$. For the first step, the HαC potential and tunneling of the α-α system is schematically depicted in Fig. 1.

In the top panel, we show the α-α potential with the two different parameterizations. Due to the approximate treatment of the Pauli correlations via a potential term, the ground state configurations are solid-like [27]. Thus, the resonance and ground states correspond to the minimum of the potentials. Both are the same after 6 fm, which suggests that the corresponding fusion cross sections will be mostly similar. In the bottom panel, we turn our attention to the potential fitted to the ^{8}Be resonance. We

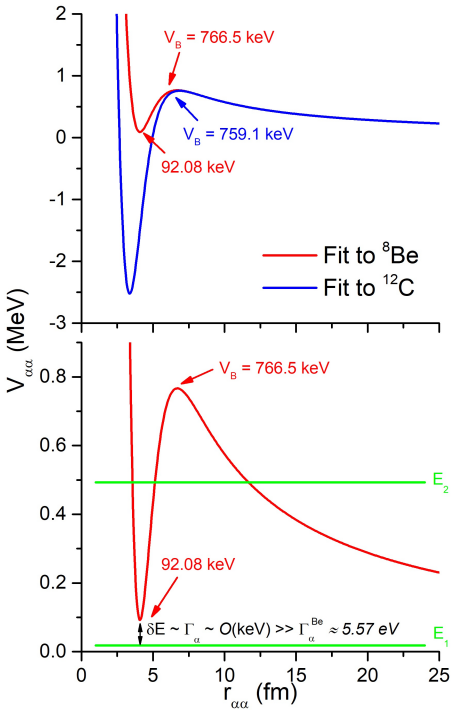

Figure 1. Top: α-α potential fitted to ^{8}Be (red) and ^{12}C (blue). Bottom: α-α potential fitted to ^{8}Be (red), along with two possible E_{CM} values (green), $E_1 < E_{^8Be} < E_2$. We denote the value of the barrier (V_B) and the energy of the resonance.

note that, for energies below the $E_{^8Be}$ threshold, there is no second turning point, i.e., the action tends to infinity and the penetrability to zero. Quantum-mechanically, energy conservation can be violated according to the Heisenberg principle. Beryllium can then be formed even for energies below the threshold, but with a lifetime of at most $O(keV) \sim O(10^3 fm/c)$, which is much shorter than the lifetime of the resonance, at $\sim 3.5\ 10^7$ fm/c [28]. This essentially prohibits the second step to take place, since the third α particle does not reach the intermediate beryllium, before it decays. As we discuss later, we include this feature in the calculation of the reduced rate, in contrast to previous works [4, 5, 15]. In the NACRE methodology in specific, the elastic cross section is used for the first step. This is approximated by a Breit-Wigner distribution [5]:

$$\sigma_f^N(E) = \frac{\pi}{k^2}\omega_l\frac{\Gamma_\alpha^2}{(E-E_R)^2 + (\Gamma_\alpha/2)^2}, \tag{6}$$

where ω_l is a statistical factor which includes the spins of all the participating nuclei and Γ_α is the width of the inverse α-decay. The quantity E_R refers to the resonance energy, which for the first step is equal to $E_{^8Be}$.

To formally take into account the threshold effect, the α width should have the value of the energy violation below the threshold, i.e., it must contain a term of the form $(E_{^8Be} - E)\,\theta(E_{^8Be} - E)$. Additionally, the fusion cross section must be subtracted by its resonance value, i.e., $\sigma_{f,1}(E) \rightarrow \sigma_{f,1}(E) - \sigma_{f,1}(E_{^8Be})$. The fusion cross

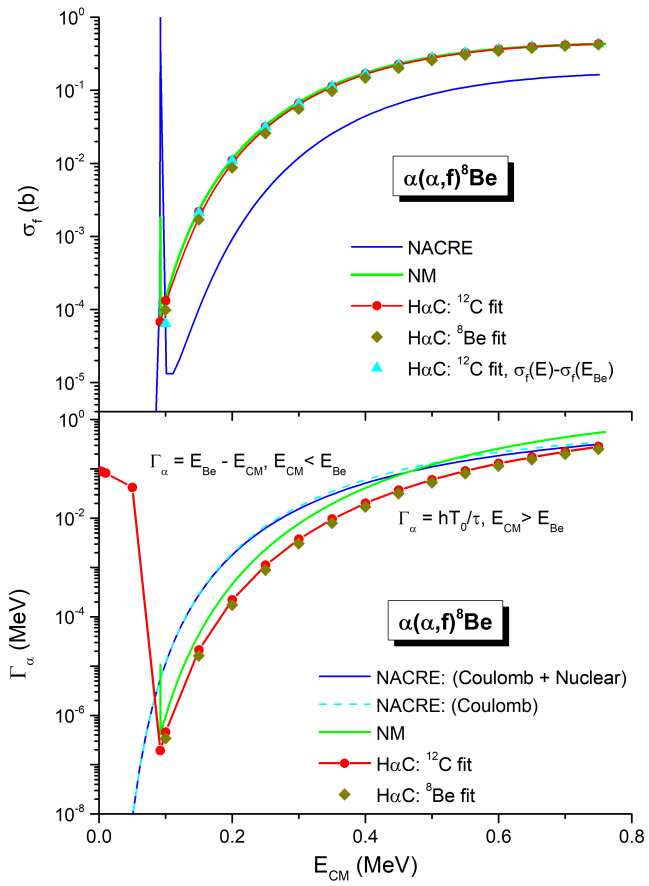

Figure 2. Top: α-α fusion cross sections obtained via the NM (green) and the several HαC schemes (points). The NACRE data are shown in blue. Bottom: Same as before for the α-decay widths of ^{8}Be. The dashed line shows the NACRE data with the penetrability obtained assuming only the Coulomb interaction. We note that the NM data start from the resonance to account for the threshold energy effect.

sections for the first step are presented in Fig. 2 (top). The blue line represents the NACRE calculations and the green to the NM results. The points correspond to the HαC calculations, with the standard parameterization (red) and the ^{8}Be fitted (brown). Furthermore, the cyan points describe the formal subtraction of the resonance cross section. We see that our initial assumption of the similarity of the cross section obtained by the different HαC schemes is observed. The NM and HαC results are also equivalent apart from the resonance peak, which is not present in the latter, due to its semi-classical nature [19]. All of our calculations are generally higher than the NACRE elastic data away from the resonance, as expected.

For the α widths of both steps above the threshold energy, we follow the approach of Refs. [29, 30] as:

$$\Gamma_\alpha = (E_{th} - E)\,\theta(E_{th} - E) + \frac{\hbar}{\tau} T_0 \theta(E - E_{th}), \quad (7)$$

where E_{th} is the threshold energy (equal to $E_{^8Be}$ for the first step and 0 for the second), T_0 is the penetrability and τ is the imaginary time interval for the system undergoing the inverse fusion process. The quantity T_0 gives the tunneling probability, while $1/\tau$ is the frequency of the α particle traversing the barrier before it returns to real time. We stress that it is not a constant, but a function of energy. In the NACRE methodology, the widths are given by [5, 8]:

$$\Gamma_\alpha^N = \Gamma_\alpha^{(0)} \frac{T_0(E)}{T_0(E_R)}. \quad (8)$$

We see that the NACRE widths are normalized to their value on the resonance, which results in higher values. Additionally, the normalization makes the width independent on the physical characteristics of system contained in the calculation of the penetrability. This is clearly depicted in Fig. 2 (bottom). The dashed cyan line corresponds to NACRE calculations, with the penetrability calculated using only the Coulomb interaction and is the same as the solid blue line, where the nuclear force is also included. Both are higher than the NM (green line) and HαC (red and brown points) data. The former is in agreement with NACRE on the resonance energy, while both HαC schemes are the same above the threshold. The increase of the width below the threshold comes from the first term in Eq. 7.

For the cross section of the 3α's second step, we follow a statistical compound nucleus approach. The reaction can be broken down into the fusion and γ or α decay components. The fusion part is handled in a similar manner to the first step reaction, taking into account the zero threshold energy and the Hoyle resonance. Then, the decay probability via α or γ is given by the branching ratio. The cross section is then, written as:

$$\sigma_2(E) = \sigma_{f,2}(E)\frac{\Gamma_{\gamma,2}}{\Gamma_2} = \sigma_{f,2}(E)\frac{\Gamma_{\gamma,2}}{\Gamma_{\alpha,2} + \Gamma_{\gamma,2}}, \quad (9)$$

with $\Gamma_2, \Gamma_{\alpha,2}$ and $\Gamma_{\gamma,2}$ being the total, α and γ widths for the ^{12}C decay, respectively. In the NACRE framework, $\sigma_2(E)$ is, again, given by a Breit-Wigner distribution [5]:

$$\sigma_2^N(E) = \frac{\pi}{k^2}\omega_l \frac{\Gamma_{\alpha,2}\Gamma_{\gamma,2}}{(E - E_R)^2 + (\Gamma_2/2)^2} \approx \sigma_{f,2}^N(E)\frac{\Gamma_{\gamma,2}}{\Gamma_{\alpha,2}}, \quad (10)$$

where in our case $E_R = E_H$, i.e, the energy of the Hoyle state and $\sigma_{f,2}^N$ is given by Eq. 6. The difference between Eq. 9 and Eq. 10 is evident. In the limit of high energies, $\Gamma_2 \approx \Gamma_{\alpha,2}$, so the two approaches yield similar results. At lower energies though, the approximation is not valid and an increased cross section is expected.

To evaluate the γ widths, we start from the standard perturbative description [31]:

$$\Gamma_\gamma = \frac{8\pi(L+1)}{L[(2L+1)!!]^2}\left(\frac{E_\gamma}{\hbar c}\right)^{2L+1} B(E_I; L). \quad (11)$$

The L-value refers to the angular momentum of the photon, which for our case is $L = 2$ and $E_\gamma = E_I - E_F$ is its energy, with E_I and E_F being the energies of initial and final compound nucleus states, respectively. The quantity

$B(E_I; L)$ is the reduced nuclear matrix element for the transition and depends on the characteristics of the initial state. Eq. 11 can be simplified by normalizing it with the value of the width at the resonance energy $\Gamma_\gamma^{(0)} = \Gamma_\gamma(E_R)$:

$$\Gamma_\gamma = \Gamma_\gamma^{(0)} \left(\frac{E_I - E_F}{E_R - E_F} \right)^{2L+1} \frac{B(E_I; L)}{B(E_R; L)}. \quad (12)$$

Usually in the literature [5, 6, 8, 16] , it is assumed that the nuclear matrix element has the approximately same value in the entire energy range, i.e., $B(E_I; L) \approx B(E_R; L)$ and thus:

$$\Gamma_\gamma^N = \Gamma_\gamma^{(0)} \left(\frac{E_I - E_F}{E_R - E_F} \right)^{2L+1}. \quad (13)$$

This approximation is quite substantial, the nuclear characteristics are different near a resonant state and in the continuum [31]. In contrast, for a discrete state, the nuclear matrix elements should have a global functional form for all its possible decay paths, as they stem from the same nucleon-nucleon interaction. Thus, we may approximate the last factor in Eq. 13 via the ratio of the α widths. The γ widths are then calculated via the expression:

$$\Gamma_\gamma = \Gamma_\gamma^{(0)} \left(\frac{E_I - E_F}{E_R - E_F} \right)^{2L+1} \frac{\Gamma_\alpha(E_I - Q)}{\Gamma_\alpha^{(0)}}, \quad (14)$$

where Q is the Q-value for the reaction, which in our case is $Q = Q_2 = 7.3667$ MeV [28] for the second step. The cross section for the second step of the 3α process calculated via the several different approaches is shown in Fig. 3.

The bottom panel shows the cross section of the second step reaction with the beryllium in its ground state. The NM (green) and HαC (red) results are once more similar apart from the resonance. We also show the original NACRE data (blue) and data obtained via the NACRE formalism, but with the corrected Γ_γ/Γ branching ratio. The two curves are virtually the same for energies above 250 keV, as expected. Due to its short lifetime, beryllium-8 reacts with the α particle having excitation energy, equal to the center of mass energy of the two fusing α particles from the first step, i.e., $E^*_{^8Be} = E_{\alpha\alpha}$. Nevertheless, the dependence of the cross section to the excitation energy is weak, as we show in Fig. 3 (top). There, we plot the HαC model cross sections for the second step with $E^*_{^8Be} = 100$ keV, 500 keV and 750 keV excitation energies divided by the corresponding ground state cross sections. It can be seen that for excitation energies below the Coulomb barrier of the first step (which is at 766.5 keV), the cross section can vary by at most a factor of 3. As we discuss below, this discrepancy is rather small for the calculation of the reaction rates which varies for almost 45 orders of magnitude. In that sense, we are permitted to use the ground state cross sections for the calculation of the reaction rate, up to a good approximation.

At this point, we are able to combine our results of the cross sections and widths to obtain the reduced reaction rate, as the main observable for an astrophysical scenario. Following the kinematics of the sequential channel, the reduced rate is given by [5]:

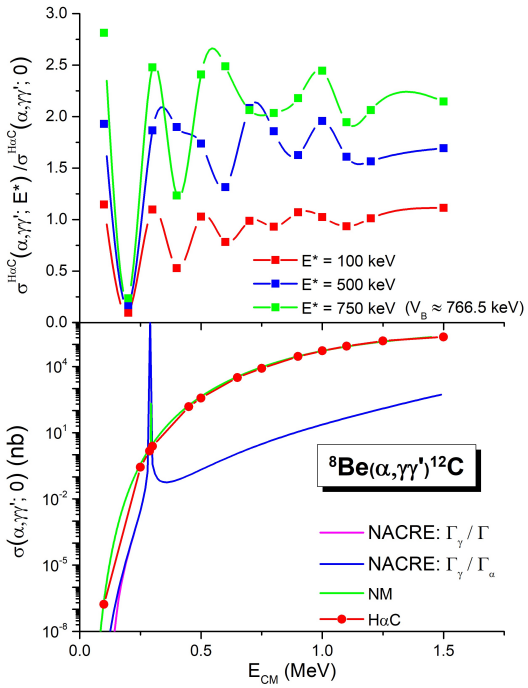

Figure 3. Top: Cross section for the second step reaction for $E^*_{^8Be} = 100$ keV, 500 keV and 750 keV calculated via the HαC model, normalized by the $E^*_{^8Be} = 0$ keV data. The maximum beryllium excitation energy is $V_B = 766.5$ MeV. Bottom: Cross section for the second step with ^{8}Be in the ground state calculated via the NM (green), HαC (red), the NACRE original framework (blue) and the NACRE with the branching width correction (purple).

$$\langle \alpha\alpha\alpha \rangle = 3 \sqrt{\frac{8\pi}{\mu_{\alpha\alpha} (kT)^3}} \int_{E_{low}}^{E_{high}} \frac{\hbar\sigma_{f,1}}{\Gamma_{\alpha,1}} \langle \sigma_2 v \rangle e^{-E/kT} E dE, \quad (15)$$

with $\mu_{\alpha\alpha}$ being the reduced mass and E the energy of the α-α system. The factor $\langle \sigma_2 v \rangle$ signifies the reduced reaction rate for the second step. Although in principle it is a function of the beryllium excitation energy E, we take this as a constant with minor discrepancies, as we discussed before. This quantity is given by [5]:

$$\langle \sigma_2 v \rangle = \sqrt{\frac{8\pi}{\mu_{\alpha Be} (kT)^3}} \int_0^{V'_B} \sigma_2 e^{-E'/kT} E' dE', \quad (16)$$

with $\mu_{\alpha Be}$ being the reduced mass, E' the energy and V'_B the barrier energy of the α-^{8}Be system.

One main difference of our framework and the NACRE methodology is the choice of the integration limits E_{low} and E_{high} in Eq. 15. The formal subtraction of the threshold cross section that was discussed before, is equivalent to an integration starting from the threshold energy, so $E_{low} = E_{^8Be}$. Additionally, for the helium burning temperature region of $\sim$ 0.01 - 1 GK, the α-α fusion happens below the Coulomb barrier and thus,

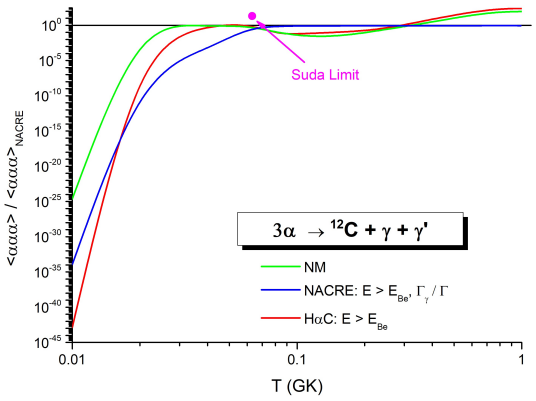

Figure 4. Reduced reaction rates obtained via the NM (green), HαC (red) and modified NACRE (blue) approaches, divided by the original NACRE data. The black line corresponds to a ratio of 1. With purple point we denote the astrophysical limit that was set by Suda [14].

$E_{high} = V_B \approx 766.5$ keV. On the contrary, in the NACRE formulation [5], the integration takes place from zero to infinity, disregarding the threshold energy. A similar situation is also present for the reduced rate of the second step (Eq. 16), where the lower integration limit is the same for both approaches, while the higher is again take at infinity by the NACRE group.

The consequences of the aforementioned choices are substantial for the reduced rates, as is presented in Fig. 4. The ratio of the rates of different formulations divided by the original NACRE data [5] is plotted as a function of the stellar temperature. The green line corresponds to the NM calculations and the red to the HαC data. We note that due to the similarity of the cross sections and widths that is shown in Fig. 1, the different HαC parameterizations yield equivalent results. The blue curve shows the results of the NACRE method, modified such as, the integration to start from the threshold and the total width being used in the denominator of the branching ratio. For $T \sim 0.1$ GK that the majority of the helium burning takes place, all approaches have results close to those of NACRE, i.e., their ratio is almost unity. On the contrary, in the 0.01 GK region, the original NACRE rates are enhanced by on average 35 orders of magnitude, in comparison to our results. Similarly high values are also obtained by some direct 3-Body approaches [6, 7, 9, 10, 32, 33], while the calculations of Refs. [6, 7] are enhanced several order of magnitude when compared to the NACRE data. These significant discrepancies, may seriously affect the early dynamics of stars, as helium burning may start at an earlier point of the star's life, when $T < 10^{7.6}$-10^{8} K [14]. We also point out that, the HαC data are lower than the rest, due to the lack of resonances, while the NM yields the highest values, because of them.

In Fig. 4 we also include an astrophysical upper limit by Suda *et. al* [14]. This sets an upper bound for the reduced rate at $T \sim 10^{7.8}$ K to the value of 10^{-29} cm^{6}s^{-1}. The limit is set for the simulated and observed luminosities of the First Asymptotic Giant Branch stars to be in agreement. The upper bound is above the ratio value of 1, so it is obeyed by both NACRE and our results, while it excludes some of the direct 3-Body approaches [6, 7]. These could affect significantly the low temperature region. Other direct 3-body approaches apply a renormalization in the helium burning temperature region, such that they reproduce the NACRE results [9, 10, 32, 33], which puts their predictive power into question. Consequentially, more limiting constraints are required for the 3α rates, which they could originate from the point of view of nuclear physics. By employing the Trojan Horse Method (THM) [34], experimental studies could mostly bypass the small lifetime of beryllium-8 and the reduction of the cross section due to Coulomb interaction, via the use of a heavier clusterized composite nucleus.

To summarize, in this work we study the sequential channel of the 3α process, by proposing a novel theoretical framework. Our methodology is based on the semi-classical Hybrid α-Clustering and Neck models, coupled with the Imaginary Time Method. The mathematical structure of our model presents a re-evaluation of the widely used NACRE method, due to the effect of the Heisenberg Principle's constraint on the threshold energy, as well as the way the decay widths are taken into account. Our results differ by on average 35 orders of magnitude in the low temperature region, albeit being similar for higher temperatures. This might have crucial implications for the early stellar dynamics of systems after the main sequence, while obey the astrophysical constraints set by Suda *et. al*. This stresses the need for stringer constraints from nuclear reaction experiments and a detailed revisit of the theory of other possible helium burning mechanisms.

This work was supported in part by the United States Department of Energy under Grant #DE-FG03-93ER40773 and by the National Natural Science Foundation of China (Grant Nos. 11905120 and 11947416).

References

[1] C.W. Cook, W. Fowler, C. Lauritsen, T. Lauritsen, Phys. Rev. **107**, 508 (1957).
[2] F. Hoyle, Astrophys. J. Suppl. **1**, 121 (1954).
[3] E.E. Salpeter, Astrophys. J. **115**, 326 (1952).
[4] K. Langanke, M. Wiescher, F. Thielemann, Z. Physik A - Atomic Nuclei **324**, 147–152 (1986).
[5] C. Angulo, M. Arnould, M. Rayet, P. Descouvemont, D. Baye, C. Leclercq-Willain, A. Coc, S. Barhoumi, P. Aguer, C. Rolfs et al., Nuclear Physics A **656**, 3 (1999).
[6] K. Ogata, M. Kan, M. Kamimura, Progress of Theoretical Physics **122**, 1055 (2009).
[7] E. Garrido, R. de Diego, D. Fedorov, A. Jensen, Eur. Phys. J. A **47**, 102 (2011).

[8] Y. Xu, K. Takahashi, S. Goriely, M. Arnould, M. Ohta, H. Utsunomiya, Nuclear Physics A **918**, 61 (2013).
[9] N.B. Nguyen, F.M. Nunes, I.J. Thompson, Phys. Rev. C **87**, 054615 (2013).
[10] H. Suno, Y. Suzuki, P. Descouvemont, Phys. Rev. C **94**, 054607 (2016).
[11] C. Hayashi, R. Hōshi, D. Sugimoto, Progress of Theoretical Physics Supplement **22**, 1 (1962).
[12] C.E. Rolfs, W.S. Rodney, Cauldrons in the cosmos: Nuclear astrophysics (University of Chicago press, 1988)
[13] C. Iliadis, Nuclear Physics of Stars (Wiley, Weinheim, 2007)
[14] T. Suda, R. Hirschi, M. Fujimoto, The Astrophysical Journal **741**, 61 (2011).
[15] K. Nomoto, F.K. Thielemann, S. Miyaji, Astron. Astrophys. **149**, 239 (1985).
[16] J. Bishop, G.V. Rogachev, S. Ahn, E. Aboud, M. Barbui, A. Bosh, J. Hooker, C. Hunt, H. Jayatissa, E. Koshchiy et al., Phys. Rev. C **103**, L051303 (2021).
[17] H. Zheng, A. Bonasera, Symmetry **13**, 1777 (2021).
[18] A. Bonasera, G. Bertsch, E. El-Sayed, Phys. Lett. B **141** (1984).
[19] T. Depastas, S.T. Sun, H. Zheng, A. Bonasera, Phys. Rev. C **108**, 035806 (2023).
[20] R. Bass, Phys. Rev. Lett. **39**, 265 (1977).
[21] A. Bonasera, Phys. Rev. C **34**, 740 (1986).
[22] A. Bonasera, EPJ Web Conf. **252**, 05001 (2021).
[23] A. Bonasera, V. Kondratyev, Phys. Lett. B **339**, 207 (1994).
[24] V. Kondratyev, A. Bonasera, A. Iwamoto, Phys. Rev. C **61**, 044613 (2000).
[25] S. Kimura, A. Bonasera, Phys. Rev. C **76**, 031602 (2007).
[26] A. Bonasera, J.B. Natowitz, Phys. Rev. C **102**, 061602 (2020).
[27] A. Bonasera, F. Gulminelli, J. Molitoris, Physics Reports **243**, 1 (1994).
[28] M. Basunia, A. Chakraborty, Nucl. Data Sheets **186** (2022).
[29] S. Gurvitz, Phys. Rev. A **38**, 1747 (1988).
[30] M. Büttiker, R. Landauer, Phys. Rev. Lett. **49**, 1739 (1982).
[31] P. Ring, P. Schuck, The nuclear many-body problem (Springer-Verlag, New York, 1980)
[32] S. Ishikawa, Phys. Rev. C **87**, 055804 (2013).
[33] T. Akahori, Y. Funaki, K. Yabana, Phys. Rev. C **92**, 022801 (2015).
[34] A. Tumino, C. Spitaleri, M.L. Cognata, S. Cherubini, G.L. Guardo, M. Gulino, I.I. S. Hayakawa, L. Lamia, H. Petrascu, R.G. Pizzone et al., Nature **557**, 687–690 (2018).